Journal of Materials Chemistry A

PAPER

View Article Online
View Journal | View Issue

Cite this: J. Mater. Chem. A, 2016, 4, 14781

Commercial Dacron cloth supported $Cu(OH)_2$ nanobelt arrays for wearable supercapacitors†

Shuijin Lei,‡[ab] Yan Liu,‡[b] Linfeng Fei,[b] Ruobing Song,[b] Wei Lu,[b] Longlong Shu,[a] Chee Leung Mak,*[b] Yu Wang*[a] and Haitao Huang*[b]

Received 3rd August 2016
Accepted 30th August 2016

DOI: 10.1039/c6ta06634h

www.rsc.org/MaterialsA

Wearable supercapacitors have attracted considerable research interest in recent years. However, most of the wearable supercapacitors reported are either in the form of fibers or based on carbon cloth which have to be knitted into commercial cloth for wearable applications. Here we report the growth of $Cu(OH)_2$ nanobelt arrays directly on commercial Dacron cloth which serves as a positive electrode for supercapacitors. The as-prepared electrode has a high specific capacitance of 217 $mF \cdot cm^{-2}$ at a current density of 0.5 $mA \cdot cm^{-2}$ with a capacitance retention of 90% at a current density of 2 $mA \cdot cm^{-2}$ after 3000 charge/discharge cycles. A flexible all-solid-state asymmetrical supercapacitor is fabricated by sandwiching the Dacron cloth supported $Cu(OH)_2$ nanobelt arrays (positive electrode) between two carbon nanofiber matrices (negative electrodes), using KOH-PVA gel as the electrolyte and as the separator. A high areal capacitance of 195.8 $mF \cdot cm^{-2}$ at a current density of 1 $mA \cdot cm^{-2}$ can be achieved. The textile supercapacitor exhibits an energy density of 3.6×10^{-2} $mWh \cdot cm^{-2}$ at a power density of 0.6 $mW \cdot cm^{-2}$ with a voltage window of 1.2 V. This sandwich type of supercapacitor based on commercial Dacron cloth opens a novel way of integrating supercapacitors into textiles, showing great promise for wearable electronic applications.

Introduction

Wearable energy storage devices are of particular interest in modern electronics due to their advantages such as being thin, lightweight, flexible, and portable, which have potential applications in military garment devices, sportswear, and health monitoring devices. Flexible supercapacitors have been extensively investigated to explore novel next-generation energy storage, with one-dimensional (fiber or yarn) or two-dimensional (planar) architectures.[1–4] Fiber or yarn type flexible supercapacitors can be woven or knitted directly into a textile, or stitched into an existing fabric, which are attractive for realizing miniaturized portable devices and multi-functional smart textiles.[5,6] Planar-type flexible supercapacitors are mostly built on metal sheets, plastics, papers, and carbon cloth substrates. However, these substrates are generally not suitable for integration into clothing and hence cannot effectively meet the wearable requirements.[3,7] Therefore, it is rather imperative that commercial textiles can be directly employed as a substrate to fabricate flexible and wearable supercapacitors. It is known that, apart from its thinness, flexibility, light weight and stretchability, cloth possesses a 3D porous structure, which allows a high areal mass loading of active materials and therefore high areal power and energy densities of the devices can be expected.[8] Researchers have fabricated high performance supercapacitors by coating various carbon materials (*e.g.* activated carbon, carbon nanotubes, and graphene) onto cotton or polyester textiles (either woven, knitted or non-woven) using dip-coating, screen-printing, and painting methods to incorporate these materials into fabrics.[1,9–11] However, coating of other active materials onto textile fibers is indispensable in order to construct high energy density asymmetric supercapacitors. Huang *et al.* have fabricated hierarchical PPy@MnO_2@rGO-deposited conductive yarns, which exhibited excellent specific capacitances and high energy density. These flexible all-solid-state supercapacitor yarns could be woven into large energy storage textiles and knitted into a woollen wrist band to form a pattern, enabling their wearability.[12] In this work we choose commercially available Dacron to construct the asymmetric supercapacitor due to its good strength, flexibility, thermoplasticity, glossiness, wear resistance, shrinkage resistance, chemical resistance, light resistance, low cost, consistency in quality and ready availability.[7,13]

It is well-known that one-dimensional nanostructures (nanowires, nanobelts, nanorods, nanotubes, nanocables, *etc.*) can act as superhighways for fast ion and electron transport

[a]School of Materials Science and Engineering, Nanchang University, Nanchang, Jiangxi 330031, China. E-mail: wangyu@ncu.edu.cn

[b]Department of Applied Physics, The Hong Kong Polytechnic University, Hong Kong SAR, China. E-mail: apaclmak@polyu.edu.hk; aphhuang@polyu.edu.hk

† Electronic supplementary information (ESI) available: Photograph of Cu-plated Dacron cloth, EIS of the positive electrode and supercapacitor device, and the rolling test of the device. See DOI: 10.1039/c6ta06634h

‡ These authors contributed equally to this work.

along their longitudinal direction which results in a reduction of internal resistance and an increase of rate performance for application in electrochemical energy storage devices. Additionally, they can offer a large surface area, endure large volume changes, and exhibit good strain accommodation.[14,15] To date, for the flexible supercapacitors based on 1-D nanoarrays, the active materials are normally built on conductive substrates, such as metal sheets, metal foils, carbon cloth and carbon paper.[16–20] It is still a great challenge to deposit these capacitive materials directly on fabrics. Although metal coated polymer substrates, such as Ni-coated cotton yarns, have been applied in energy related devices,[21–23] it would be significant to use commercial cloth as a substrate to scaffold metal oxides or hydroxides for supercapacitors. Among many transition metal oxides and hydroxides, copper-based materials (including CuO, $Cu(OH)_2$, Cu_2O, *etc.*) have attracted much attention as pseudocapacitor electrode materials because they are chemically stable, of low cost, and environmentally friendly.[24–29] Particularly, using $Cu(OH)_2$, Gurav *et al.* have synthesized $Cu(OH)_2$ films on glass and stainless steel substrates,[27] and Xu *et al.* have fabricated $Cu(OH)_2$ nanowire arrays on copper foil.[28] However, it is obvious that these substrates are not suitable for constructing wearable devices.

In this work, $Cu(OH)_2$ 1D nanostructured arrays were directly grown on Cu-coated commercial Dacron cloth and used as a pseudocapacitive material. To the best of our knowledge, there is no available report on the use of commercial cloth as a substrate to scaffold metal oxides or hydroxides for supercapacitors. In our approach, copper was first electro-plated on Dacron cloth, where each single fiber of the cloth was uniformly coated with a layer of copper to form a conducting network. Such Cu-plated cloth has excellent mechanical properties and the cloth can be washed more than ten times without losing its electrical conductivity (~0.02 Ω/sq). Therefore the Cu-plated cloth was used as a current collector for the supercapacitor in the following study. $Cu(OH)_2$ 1D nanostructured arrays were then *in situ* grown on the copper-plated cloth by treatment in ammonia solution. Subsequently, a sandwich-type asymmetric all-solid-state supercapacitor was assembled using the as-prepared $Cu(OH)_2$ 1D nano-arrays and carbon nanofibers (CNFs) as the positive and negative electrodes, respectively, and KOH-PVA gel as the electrolyte and also as the separator. The schematic diagrams and the corresponding photographs of the commercial Dacron cloth, copper-plated cloth, $Cu(OH)_2$ coated cloth, and supercapacitor device are shown in Fig. 1. The electrochemical properties of the Dacron cloth supported $Cu(OH)_2$ electrodes were investigated both in aqueous electrolytes and in the solid-state device. The as-developed solid-state supercapacitor has demonstrated high areal capacitance, high energy density, and good rate capability, as well as good cycling and bending stability, making it promising as an energy storage device that can be easily integrated into commercial textiles. This research would also be desirable to broaden the range of materials and reduce the cost of supercapacitors.

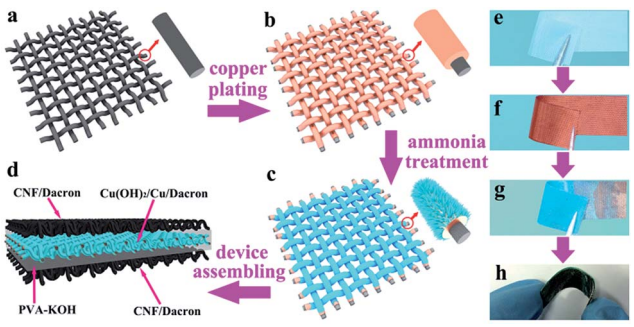

Fig. 1 Schematic diagrams and the corresponding photographs of (a, e) the pristine Dacron cloth, (b, f) copper-plated cloth, (c, g) $Cu(OH)_2$ coated cloth, and (d, h) supercapacitor device.

Experimental

Preparation of copper-plated Dacron cloth

Commercial Dacron cloth was used as the flexible substrate in this study (Fig. 1a and e). It was metallized by employing nickel electroless-plating and copper electro-plating methods. Before plating, the cloth was cut into a given size and cleaned with detergent in an ultrasonic bath to remove grease and/or dirt. The cleaned cloth was dipped into 4 M NaOH for 30 minutes to modify the surface, and then dipped into 1% HCl for 30 seconds to neutralize excess NaOH. For surface activation, the cloth was immersed into an activator solution consisting of MACuPlex activator D-34C (Macdermid, solution of Pd/Sn^{2+} colloidal), deionized water, 32% HCl, and sensitizer-78 for 3 minutes. The activation process should be free from air, light and water in order to avoid the oxidation and hydrolysis of Sn^{2+} ions. Subsequently, the cloth was dipped in 50 $g \cdot L^{-1}$ H_2SO_4 at 50 °C for 1 minute to remove Sn^{2+} ions. Electroless Ni plating was carried out by dipping the cloth into a MACuplex J-64 Ni bath, a mixture of deionized water, 28% NH_4OH, MACuPlex J-60 and MACuPlex J-61, at 35 °C for 3 minutes to deposit a Ni layer on the fabric. Then, the sample was further cleaned by electrolytic degreasing for 3 minutes. Finally, a standard noncyanide alkaline bath was used for electroplating of copper at 50 °C for 3 minutes. Then the copper-plated Dacron cloth can be obtained, which still exhibits very good flexibility (Fig. 1f). It should be noted that after each step the cloth should be thoroughly rinsed with deionized water for a while to remove residues on the surface.

Growth of $Cu(OH)_2$ nanobelt arrays on Dacron cloth

A piece of the as-prepared copper-plated Dacron cloth was cleaned by rinsing in absolute ethanol, 4 M hydrogen chloride aqueous solution and deionized water for several minutes, consecutively, and dried in a vacuum. The cleaned copper-plated Dacron cloth was then vertically and partly immersed into a diluted ammonia aqueous solution (0.03 M) in a glass reactor. In order to prevent the unsubmerged part of the cloth from reacting with the solution, a trace of Vaseline was smeared on the cloth over the solution to prevent capillarity. The reactor was sealed with parafilm keeping the unsubmerged part of the cloth outside the reactor. The slit for passing of the cloth on the

parafilm was also sealed with Vaseline. The unreacted part of the copper-plated cloth can thus serve as the conductor of the later fabricated supercapacitor devices. Subsequently, the reactor was placed in a refrigerator (2–5 °C) for 2–3 days and a blue thin film appeared on the surface of the cloth, indicating the formation of $Cu(OH)_2$ (Fig. 1c and g). Finally, Vaseline on the cloth was carefully removed using toluene. It was then washed by immersing successively in deionized water and absolute ethanol and dried in air for use.

Preparation of the CNF electrode

Carbon nanofibers were synthesized by electrospinning of polyacrylonitrile (PAN), followed by stabilization and carbonization.[30] To fabricate the CNF electrode, a homogeneous slurry was first prepared by mixing 80 wt% porous carbon nanofibers as the active material, 10 wt% acetylene black as the conductive agent, and 10 wt% polyvinylidene fluoride as the binder in 1-methyl-2-pyrrolidinone solvent. Dacron cloth was then immersed into the slurry to load CNFs. The CNF-coated Dacron cloth was taken out of the slurry and dried at 60 °C for 24 h, forming the CNF/Dacron electrode.

Fabrication of the all-solid-state supercapacitor

The poly(vinyl alcohol) (PVA)-KOH gel electrolyte was prepared as follows: in a typical process, 2 g of PVA was dissolved in 20 mL deionized water under continuous stirring at 90 °C for 2 h. A clear viscous solution was obtained. After it was cooled down to ambient temperature, KOH aqueous solution was slowly dropped into the viscous solution with sufficient stirring until the solution became clear. The sandwich structured device was assembled in the following way: the as-prepared $Cu(OH)_2$/Cu/Dacron and CNF/Dacron electrodes were soaked in the hot PVA-KOH gel electrolyte (50–60 °C) for 10 min and then hung for 15 min under ambient conditions to allow the electrolyte to diffuse into the nanoporous structure of active materials. This coating process was repeated three times. Then the $Cu(OH)_2$/Cu/Dacron electrode was sandwiched between two CNF/Dacron electrodes by pressing against each other and dried in hot air until the gel electrolyte was solidified with the evaporation of water. Silver paste was used for electric contact between the carbon fiber cloth and instrument. The as-fabricated all-solid-state asymmetric supercapacitor can be labeled as CNF/Dacron ‖ $Cu(OH)_2$/Cu/Dacron ‖ CNF/Dacron.

Material characterization

X-ray powder diffraction (XRD) patterns were recorded on a Rigaku SmartLab Intelligent X-ray diffraction system with filtered Cu Kα radiation ($\lambda = 1.5406$ Å, operating at 45 kV and 200 mA). Scanning electron microscopy (SEM) was preformed on a JEOL-6490 scanning electron microscope at an acceleration voltage of 20 kV. Field-emission scanning electronic microscopy (FE-SEM) observations were carried out on a JEOL-6335F field-emission system. Transmission electron microscopy (TEM) images and selected area electron diffraction (SAED) patterns were taken from a JEM-2100F (field emission) scanning transmission electron microscope (JEOL, Japan) at an acceleration voltage of 200 kV. The sample grown on the Cu-plated cloth substrate was directly used for the XRD and SEM tests. For TEM tests, the sample was detached from the substrate and dispersed in ethanol by ultrasonication, followed by drying on an amorphous carbon film supported copper grid.

Electrochemical characterization

Cyclic voltammetry (CV), galvanostatic charge/discharge (GCD), and electrochemical impedance spectroscopy (EIS) of individual electrodes ($Cu(OH)_2$/Cu/Dacron and CNF/Dacron) were performed on a CHI 660E electrochemical workstation (Chenhua, China) using a classical three-electrode configuration in 1 M NaOH aqueous electrolyte. Platinum and saturated calomel electrodes were used as counter and reference electrodes, respectively. EIS measurements were performed by applying an alternating voltage with an amplitude of 5 mV in a frequency range from 10 mHz to 10 kHz at the open circuit potential.

Results and discussion

Structural characterizations

Fig. 2a shows the morphology of the pristine Dacron cloth at low magnification. It can be seen that the cloth is well woven. The high magnification SEM image (Fig. 2b) shows that the cloth has a smooth surface and the individual fiber has a diameter of about 15 μm. After copper-plating, it is obvious that the original woven structure was well maintained (Fig. 2c and d). Although some small cracks on the surface (marked by arrows) are visible, each fiber is fully covered by the Cu coating layer. Moreover, the flexibility is also preserved as shown in Fig. 1f. The obtained

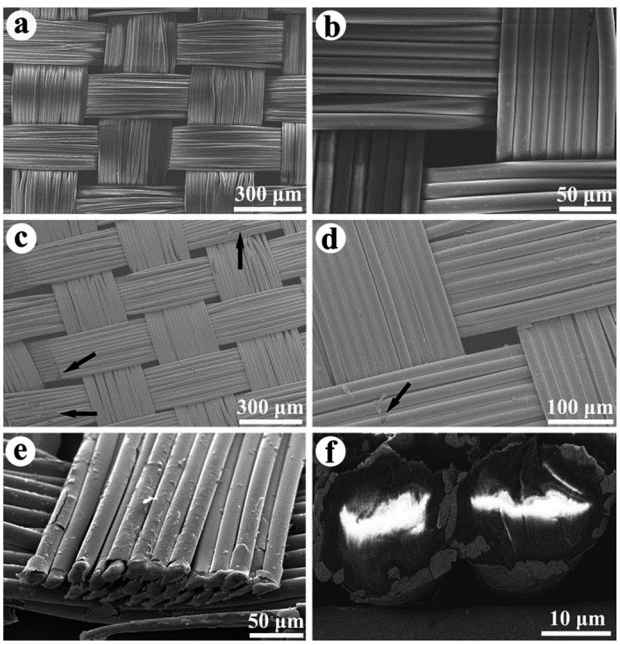

Fig. 2 SEM images of the commercial Dacron cloth at (a) low and (b) high magnifications. SEM images of the copper-plated Dacron cloth at (c) low and (d) high magnifications. Cross-sectional SEM images of the copper-plated Dacron cloth at (e) low and (f) high magnifications.

Cu-plated cloth can be even violently kneaded without significant damage to the Cu coating layer showing its good adhesion to the cloth fiber.[31] A core@shell coaxial cable-like structure is clearly visible in the cross-sectional SEM images of the copper-plated sample (Fig. 2e), with the cloth fiber as the core and the Cu layer as the shell. The enlarged SEM micrograph (Fig. 2f) confirms that a Cu layer is uniformly coated on every single fiber, with a thickness of around 0.6 μm. Also, the photograph of a large piece of the Cu-plated Dacron cloth is shown in Fig. S1 (ESI†).

After aqueous ammonia treatment, a green coating can be formed on the surface of the Cu-plated cloth (Fig. 1c and g). To identify the phase composition of the coating, X-ray diffraction (XRD) was performed and the resulting patterns are shown in Fig. 3. The diffraction peaks located at 43.4° and 50.5° are derived from the residual Cu layer (fcc-Cu, JCPDS Card File No. 89-2838). The residual Cu layer on the cloth ensures a good conductivity of the as-treated cloth and acts as the current collector in supercapacitor devices. The other diffraction peaks can be readily indexed to the orthorhombic $Cu(OH)_2$ with calculated lattice constants of $a = 2.948$ Å, $b = 10.602$ Å and $c = 5.251$ Å, in perfect agreement with the standard values (JCPDS Card File No. 80-0656, $a = 2.947$ Å, $b = 10.590$ Å and $c = 5.256$ Å). No other discernible reflection peaks derived from impurities such as CuO can be detected, indicating the high purity of our samples.

Fig. 4a and b show the morphology of the $Cu(OH)_2$ coating layer grown on the Dacron cloth where the sample still has the well-established texture, keeping an ordered woven structure of the Dacron cloth. Notably, the surface of each fiber is uniformly covered with regular nanostructures at a very high density. The sample still exhibits excellent flexibility (Fig. 1g) and can be readily rolled up, which makes it attractive for future flexible device applications. A close examination (Fig. 4c and d) of the $Cu(OH)_2$ coating layer shows that it is actually composed of highly ordered dense nanobelt arrays, which are vertically grown outward from the surface of each fiber. An average thickness of about 50 nm and an average width of about 500 nm

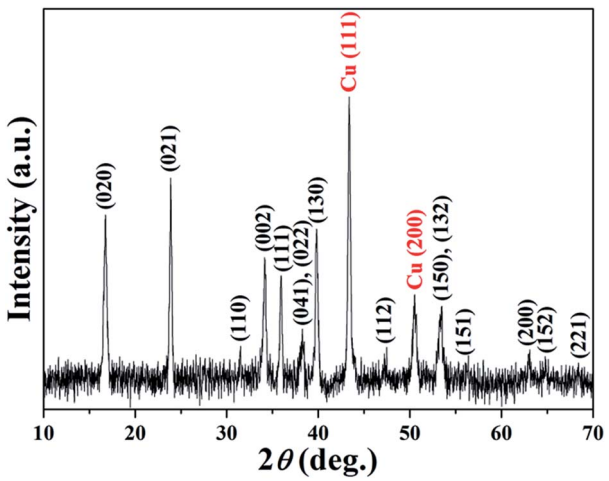

Fig. 3 XRD pattern of the as-prepared $Cu(OH)_2$ coated cloth.

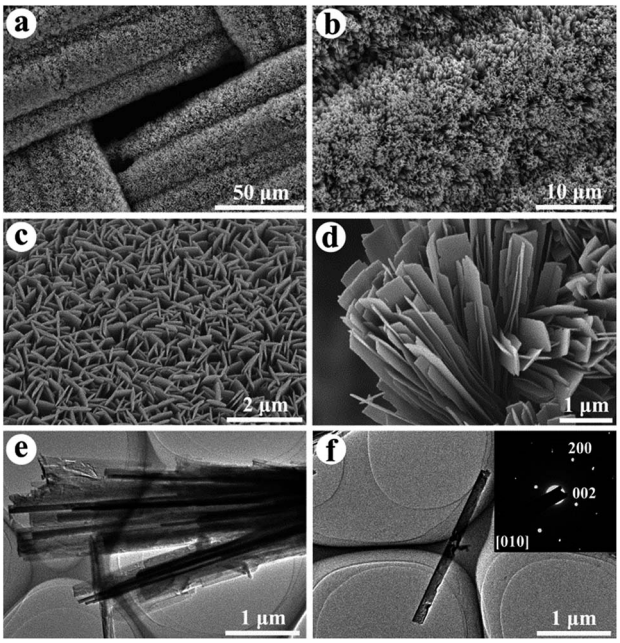

Fig. 4 (a, b) low magnification SEM images and (c, d) high magnification FE-SEM images of the as-prepared $Cu(OH)_2$ coated cloth. (e, f) TEM images of the $Cu(OH)_2$ sample detached from the cloth substrate. The inset of (f): SAED pattern of a single $Cu(OH)_2$ nanobelt taken along the [010] zone axis.

can be measured for these nanobelts. The well-aligned nanobelt array architecture implies a higher specific surface area, and thus more effective contact with the electrolyte in electrochemical devices. Fig. 4e and f further reveal the as-grown $Cu(OH)_2$ nanobelts which were detached from the cloth substrate. The belt-like nanostructures can be distinctly observed. The single crystalline feature with good crystallinity of the $Cu(OH)_2$ nanobelts can be easily confirmed from the sharp diffraction spots observed in the selected area electron diffraction (SAED) pattern (inset of Fig. 4f). The d-spacing calculation reveals that the $Cu(OH)_2$ nanobelts are orthorhombic, in good agreement with the XRD data. Furthermore, the SAED also shows that the orthorhombic $Cu(OH)_2$ nanobelts were grown along the [100] direction (*a*-axis).

Positive electrode performances

Fig. 5 shows the electrochemical properties of the obtained $Cu(OH)_2$/Cu/Dacron sample measured using a classical three-electrode configuration in 1 M NaOH aqueous electrolyte. A pair of redox peaks can be observed in the cyclic voltammetry (CV) curves (Fig. 5a), indicating a typical redox pseudocapacitance.[32] The corresponding Faradic reaction can be described as follows (eqn (1)):[28]

$$2Cu(OH)_2 + 2e^- \rightleftarrows Cu_2O + 2OH^- + H_2O \quad (1)$$

It should be noted that all these CV curves present almost the same profile, suggesting the good reversibility of the redox

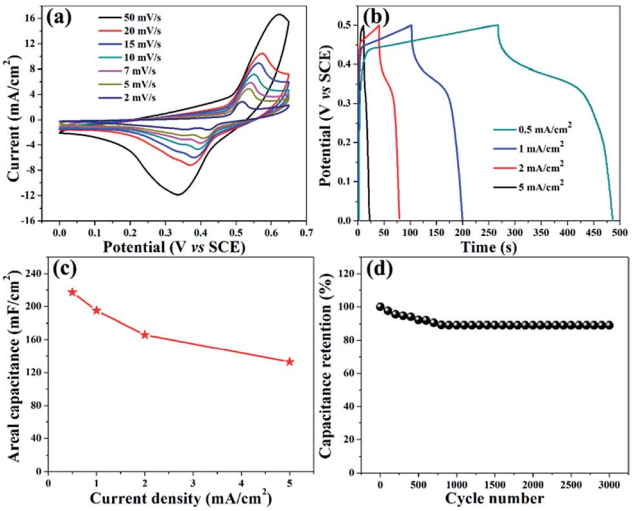

Fig. 5 (a) CV curves of the $Cu(OH)_2$/Cu/Dacron electrode at different scan rates in 1 M NaOH aqueous solution. (b) GCD curves of the $Cu(OH)_2$/Cu/Dacron electrode at different current densities. (c) The areal capacitance of the $Cu(OH)_2$/Cu/Dacron electrode as a function of current density. (d) Cycling performance of the $Cu(OH)_2$/Cu/Dacron electrode at a current density of 2 $mA \cdot cm^{-2}$ in 1 M NaOH aqueous solution.

reactions. With increased scan rates, the CV curves show higher slopes suggesting that lower scan rates enable a longer duration for the anions to access the bulk of the electrode, thereby showing ideal capacitive behavior.[28] Moreover, as the scan rate is increased, the oxidation (anodic) peak shifts to more positive potentials and the reduction (cathodic) peak shifts to more negative potentials along with increased peak separation implying the loss of reversibility, which is most probably due to the charge diffusion polarization within the electrode material.[33]

Fig. 5b shows the galvanostatic charge/discharge (GCD) measurements conducted on the $Cu(OH)_2$/Cu/Dacron electrode at different current densities. The clear plateau in the discharge curves further confirms the pseudocapacitive behavior of the electrode. The specific capacitance of the $Cu(OH)_2$/Cu/Dacron electrode at different current densities can be calculated based on the GCD curves by the following equation,

$$C = \frac{I\Delta t}{\Delta U S} \quad (2)$$

where C ($F \cdot cm^{-2}$) is the areal capacitance, I (A) is the constant discharge current, Δt is the discharge time, ΔU(v) is the potential window, and S (cm^2) is the surface area. The areal capacitances of the $Cu(OH)_2$/Cu/Dacron electrode at current densities of 0.5, 1, 2, and 5 $mA \cdot cm^{-2}$ were determined to be 217, 195, 166 and 133 $mF \cdot cm^{-2}$, respectively, as illustrated in Fig. 5c. The areal capacitance was only decreased by 39% of the initial value when the current density was increased from 0.5 to 5 $mA \cdot cm^{-2}$, suggesting the good rate capability of the $Cu(OH)_2$/Cu/Dacron electrode. Fig. 5d exhibits the cyclic stability of the electrode at a current density of 2 $mA \cdot cm^{-2}$. Within the initial 700 cycles, the areal capacitance was decreased by 10%, after which it remained almost stable at 148 $mF \cdot cm^{-2}$ up to 3000 cycles, demonstrating the excellent electrochemical stability of such electrode material.

The electrochemical impedance spectroscopy (EIS) of the $Cu(OH)_2$/Cu/Dacron electrode (Fig. S2, ESI†) shows that the Nyquist plot consists of a semicircle in the high frequency region and a straight line in the low frequency one. The high frequency intercept at the real axis is the equivalent series resistance (ESR), the diameter of the semicircle corresponds to the charge transfer resistance of the electrode, and the straight line in the low frequency region represents the Warburg resistance. The prepared $Cu(OH)_2$/Cu/Dacron electrode exhibits a small ESR value of 1.2 Ω and a low charge-transfer resistance of 1.3 Ω (inset of Fig. S2†), indicating low electrolyte resistance and low contact resistance between the active material and the current collector, which is attributed to the direct growth of $Cu(OH)_2$ on the Cu layer. The large slope of the straight line means fast ion diffusion between the electrode and electrolyte, indicating a good capacitive behavior.

Negative electrode performances

Carbon nanofibers (CNFs) have attracted great attention as energy-storage materials due to their low cost, high electroconductivity, and high specific surface area. In this work, carbon nanofibers were successfully prepared by electrospinning of polyacrylonitrile (PAN) polymer solution followed by thermal treatment and oxidation stabilization. Fig. 6a and b present the TEM images of the as-prepared CNF sample which consists of nanofibers with an average diameter of 250 nm. As judged from the SAED pattern (inset of Fig. 6b), amorphous carbon nanofibers are identified. It is well-known that the low crystallinity of the carbon nanofibers could be advantageous after activation to achieve a larger specific surface area and higher specific capacitance.[34]

The negative electrode (CNF/Dacron) was fabricated by coating CNF on Dacron cloth. Fig. 7 shows the electrochemical properties of the CNF/Dacron negative electrode measured in 1 M NaOH aqueous electrolyte. CV curves of the CNF/Dacron electrode display a quasi-rectangular shape without obvious distortion with increasing scan rates in the potential window between −1 and 0 V, indicating a typical electric double-layer capacitance behavior (Fig. 7a). GCD curves obtained at different current densities from 1 to 20 $mA \cdot cm^{-2}$ (Fig. 7b) are all symmetric triangles and no obvious IR drop can be observed, indicating the excellent electrochemical reversibility of the electrode and a very small equivalent series resistance, respectively, which are essential for high

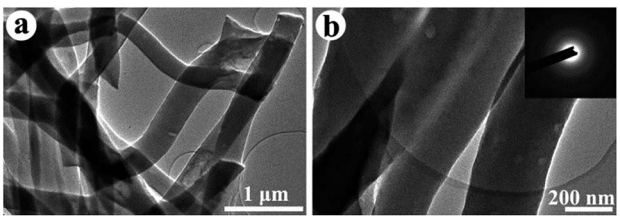

Fig. 6 TEM images of the as-prepared CNF sample at (a) low and (b) high magnifications. The inset of (b): SAED pattern of the sample.

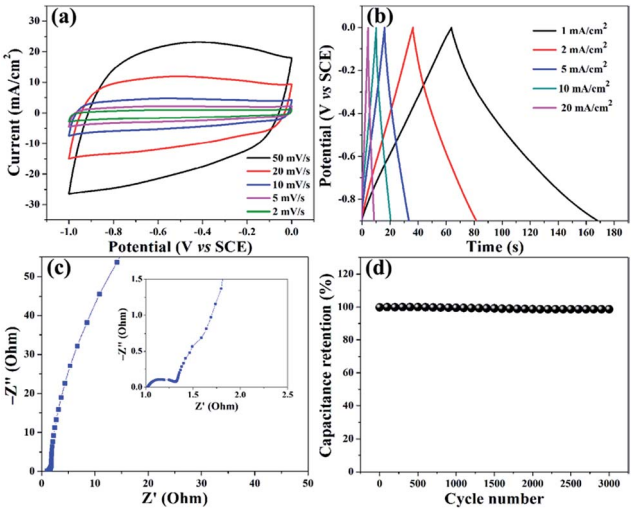

Fig. 7 (a) CV curves of the CNF/Dacron electrode at different scan rates in 1 M NaOH aqueous solution. (b) GCD curves of the CNF/Dacron electrode at different current densities. (c) Nyquist plots of the CNF/Dacron negative electrode. (d) Cycling performance of the CNF/Dacron electrode at a current density of 2 mA·cm^{-2} in 1 M NaOH aqueous solution.

power requirement of supercapacitors. The CNF/Dacron electrode exhibits a specific capacitance of 253, 245, 238, 229, and 224 mF·cm^{-2} at different current densities of 1, 2, 5, 10 and 20 mA·cm^{-2}, respectively. A high retention of 88.5% of the initial capacitance when the current density was increased by 20 times demonstrates good rate performance, which is due to fast ion transport and high conductivity.

The Nyquist plot of the CNF/Dacron electrode (in Fig. 7c) also consists of a semicircle in the high frequency region and a straight line in the low frequency region. The ESR and charge-transfer resistance are about 1.0 and 0.3 Ω, respectively. The large slope of the straight line indicates an ideal capacitive characteristic and a small ion diffusion resistance. All these results further confirm its high specific capacitance and good rate capability. Additionally, as shown in Fig. 7d, the as-prepared CNF/Dacron electrode exhibits a superior cycle life with a capacitance retention of 98.7% after 3000 charge/discharge cycles. These results demonstrate that the CNF/Dacron electrode possesses good capacitance and rate capability, suitable for the subsequent supercapacitor application.

Asymmetric all-solid-state supercapacitors

Compared to supercapacitors using liquid electrolytes, all-solid-state devices have many desirable advantages, such as a small size, light weight, high reliability, good scalability, ease of handling, improved safety and flexibility, and a wider range of operating temperature. In this perspective, all-solid-state supercapacitors hold great promise as energy storage units for flexible and wearable electronics. To further explore the advantages of this novel design for real applications, a flexible all-solid-state asymmetric supercapacitor (denoted as FASC) was assembled using the as-prepared $Cu(OH)_2$/Cu/Dacron as the positive electrode and CNF/Dacron as the negative electrode, with a solid-state gel electrolyte sandwiched in between, as illustrated in Fig. 1d. The fabricated device can be easily bent as shown in Fig. 1h. Fig. 8a compares the CV curves of the positive and negative electrodes at a scan rate of 2 mV·s^{-1}. Generally, since the operating potential windows for $Cu(OH)_2$/Cu/Dacron and CNF/Dacron electrodes are 0–0.65 V and −1–0 V, respectively, the FASC device would be expected to work in the combined window of 1.65 V. Considering the overpotential of hydrogen evolution on the electrode, the maximal voltage window may be affordable at 1.65 V, although it exceeds the theoretical limit of water electrolysis (1.23 V).[35] However, due to the serious oxygen evolution at 1.65 V, the voltage window was lowered to 1.2 V. To obtain an optimized supercapacitor performance, the charges (Q) on both electrodes should be balanced according to the following equations:[36]

$$Q^+ = Q^- \quad (3)$$

$$Q^{\pm} = C^{\pm} \cdot \Delta E^{\pm} \cdot A^{\pm} \quad (4)$$

where C is the specific capacitance (F·cm^{-2}), + and − represent positive and negative electrodes, respectively, ΔE is the potential range during charge/discharge processes, and A is the area of the electrode.

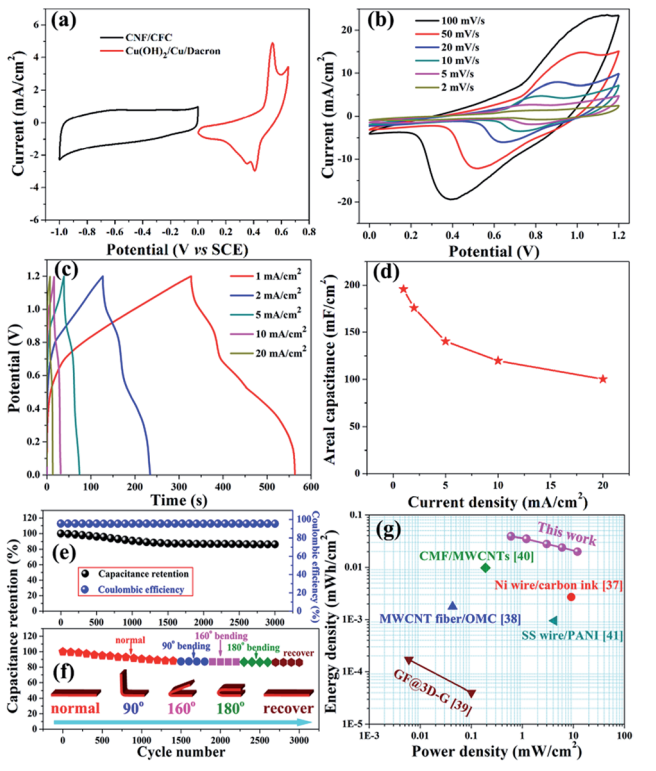

Fig. 8 (a) CV curves of the $Cu(OH)_2$/Cu/Dacron and CNF/Dacron electrodes at a scan rate of 2 mV·s^{-1}. (b) CV curves of the FASC device at different scan rates. (c) GCD curves of the FASC device at different current densities. (d) Areal capacitance of the FASC device at different current densities. (e) Cycling and (f) bending stability of the FASC device obtained by CV measurements at a scan rate of 50 mV·s^{-1}. (g) Ragone plot of the as-prepared FASC device compared with the data reported elsewhere.

Fig. 8b shows the CV curves of the assembled FASC device using KOH-PVA gel as the electrolyte at various scan rates from 2 to 50 $mV \cdot s^{-1}$. The shapes of these CV curves within a voltage window of 1.2 V remained the same, suggesting the good capacitive behavior of the device. The GCD curves of the device at different current densities are displayed in Fig. 8c and the calculated areal capacitances are 195.8, 175.6, 140.25, 119.75, and 100.3 $mF \cdot cm^{-2}$ at the current densities of 1, 2, 5, 10, and 20 $mA \cdot cm^{-2}$, respectively (Fig. 8d). These results are comparable to many previously reported values,[37–41] attractive for applications in energy-storage systems. Interestingly, it can be noted that the discharge curves exhibit two terraces at low current densities (1–2 $mA \cdot cm^{-2}$). These two terraces are related to the reduction of Cu^{2+} to Cu^{+} and finally to Cu.[42] Hence, precisely speaking, the device should be called a battery-like supercapacitor. EIS was employed to further evaluate the electrochemical performance of the FASC device (Fig. S3, ESI†). The electrolyte resistance and the charge-transfer resistance of the FASC are 1.8 and 2.7 Ω, respectively. The results suggest the relatively low resistance of the PVA-KOH solid-state electrolyte and the fast charge transfer process in the FASC device, which improves the redox activity during charging/discharging.

The cyclic test of the fabricated FASC device (Fig. 8e) shows that it can maintain 86.4% of its initial capacitance after 3000 cycles at a scan rate of 50 $mV \cdot s^{-1}$, indicating its good electrochemical performance. The Coulombic efficiency after 3000 cycles remains above 95% at a current density of 20 $mA \cdot cm^{-2}$, indicating its good charge/discharge reversibility. To verify the flexibility of the FASC device, the capacitance was measured at different bending angles in a cyclic test (Fig. 8f). It can be seen that, similar to Fig. 8e, the device shows a capacitance degradation of about 10% during the initial 1100 cycles at the normal state, and then the capacitance retention appears to be relatively stable. After 1400 cycles, the device was then tested continuously for 400 cycles each under the three consecutive bending states, 90°, 160° and 180°, at the same scan rate. Finally the device was tested in the normal state for another 400 cycles. As shown in Fig. 8f, the device still exhibits 86.1% retention of the initial capacitance after all the above 3000 cycles. Comparing Fig. 8f and e, it is clear that there is no obvious retention decrease between the devices with and without bending, indicating its excellent mechanical flexibility for practical flexible device applications. To further evaluate the flexibility of our device, a rolling test was also performed. Briefly, after rolling 20 times, the device was then tested uninterruptedly for 100 cycles. Then this process was repeated, with a total rolling number of 600 and a total cycle number of 3000. As shown in Fig. S4 (ESI†), after the continuous rolling process, the prepared FASC device still shows 82.7% retention of the initial capacitance, revealing its good mechanical flexibility and cyclic stability.

Fig. 8g compares the Ragone plot of the FASC device with some of the recently reported devices. The energy density and power density are calculated as $W = C(\Delta U)^2/(2 \times 3600)$ and $P = 3600W\ t^{-1}$, respectively, where W is the energy density ($mWh \cdot cm^{-2}$), C is the specific capacitance of the device ($mF \cdot cm^{-2}$), ΔU is the voltage window of the device (V), P is the power density ($mW \cdot cm^{-2}$), and t is the discharge time (s). The FASC device fabricated in this work delivers a maximum energy density of 3.6×10^{-2} $mWh \cdot cm^{-2}$ at a power density of 0.6 $mW \cdot cm^{-2}$ with a voltage window of 1.2 V, and 52% of the energy density can be retained as the power density is increased by 20 times to 12 $mW \cdot cm^{-2}$. The obtained energy density is significantly higher than the reported values of many flexible supercapacitors, such as Ni wire/carbon ink (2.7×10^{-3} $mWh \cdot cm^{-2}$),[37] multi-walled carbon nanotube fibers/ordered mesoporous carbon (MWCNT fibers/OMC, 1.77×10^{-3} $mWh \cdot cm^{-2}$),[38] graphene fiber/3D graphene (GF@3D-G, $<1.7 \times 10^{-4}$ $mWh \cdot cm^{-2}$),[39] carbon microfiber/multi-walled carbon nanotubes (CMF/MWCNTs, 9.8×10^{-3} $mWh \cdot cm^{-2}$),[40] and stainless steel wire/polyaniline (SS wire/PANI, 9.5×10^{-4} $mWh \cdot cm^{-2}$).[41] Therefore, the fabricated FASC device shows attractive potential for wearable electronic applications.

Conclusions

We have successfully employed commercial Dacron cloth as a substrate to support the growth of $Cu(OH)_2$ nanobelt arrays, which can be effectively used as a positive electrode in a pseudocapacitor. The $Cu(OH)_2$/Cu/Dacron electrode exhibited high areal specific capacitance (217 $mF \cdot cm^{-2}$ at 0.5 $mA \cdot cm^{-2}$) and outstanding cycle stability (90% capacitance retention after 3000 cycles). The assembled flexible all-solid-state asymmetric supercapacitor offered a high areal capacitance of 195.8 $mF \cdot cm^{-2}$ at 1 $mA \cdot cm^{-2}$ and a high energy density of 3.6×10^{-2} $mWh \cdot cm^{-2}$ at a power density of 0.6 $mW \cdot cm^{-2}$ with a voltage window of 1.2 V, where $Cu(OH)_2$/Cu/Dacron was used as the positive electrode, CNF/Dacron as the negative electrode, and KOH-PVA gel as the electrolyte. The fabricated device also had good rate capability and good cycling stability, as well as good flexibility. These remarkable performances demonstrated that such a $Cu(OH)_2$/Cu/Dacron architecture has great potential for high performance flexible and wearable supercapacitor applications.

Acknowledgements

This work was supported by the Research Grants Council of the Hong Kong Special Administrative Region, China (Project No. M-PolyU503/13 and PolyU5159/13E) and Hong Kong Polytechnic University (Project No. 1-BBA3). It was also supported by the National Natural Science Foundation of China (21461014), the Project for Young Scientist Training of Jiangxi Province (20153BCB23022), the Natural Science Foundation of Jiangxi Province (20151BAB206016), and the National High Technology Research and Development Program of China (863 Program, 2014AA020539).

Notes and references

1 L. B. Hu, M. Pasta, F. L. Mantia, L. F. Cui, S. Jeong, H. D. Deshazer, J. W. Choi, S. M. Han and Y. Cui, *Nano Lett.*, 2010, **10**, 708–714.
2 K. Jost, G. Diona and Y. Gogotsi, *J. Mater. Chem. A*, 2014, **2**, 10776–10787.

3 X. Cai, M. Peng, X. Yu, Y. P. Fu and D. C. Zou, *J. Mater. Chem. C*, 2014, **2**, 1184–1200.
4 X. F. Wang, X. H. Lu, B. Liu, D. Chen, Y. X. Tong and G. Z. Shen, *Adv. Mater.*, 2014, **26**, 4763–4782.
5 S. T. Senthilkumar, Y. Wang and H. T. Huang, *J. Mater. Chem. A*, 2015, **3**, 20863–20879.
6 D. S. Yu, Q. H. Qian, L. Wei, W. C. Jiang, K. Goh, J. Wei, J. Zhang and Y. Chen, *Chem. Soc. Rev.*, 2015, **44**, 647–662.
7 W. C. Li, C. L. Mak, C. W. Kanb and C. Y. Hui, *RSC Adv.*, 2014, **4**, 64890–64900.
8 D. P. Dubal, J. G. Kim, Y. M. Kim, R. Holze, C. D. Lokhande and W. B. Kim, *Energy Technol.*, 2014, **2**, 325–341.
9 K. Jost, C. R. Perez, J. K. McDonough, V. Presser, M. Heon, G. Dion and Y. Gogotsi, *Energy Environ. Sci.*, 2011, **4**, 5060–5067.
10 L. H. Bao and X. D. Li, *Adv. Mater.*, 2012, **24**, 3246–3252.
11 W. W. Liu, X. B. Yan, J. W. Lang, C. Peng and Q. J. Xue, *J. Mater. Chem.*, 2012, **22**, 17245–17253.
12 Y. Huang, H. Hu, Y. Huang, M. S. Zhu, W. J. Meng, C. Liu, Z. X. Pei, C. L. Hao, Z. K. Wang and C. Y. Zhi, *ACS Nano*, 2015, **9**, 4766–4775.
13 N. Pan, K. Chen, C. J. Moneg and S. Backer, *Text. Res. J.*, 2000, **70**, 502–507.
14 D. Chen, Q. F. Wang, R. M. Wang and G. Z. Shen, *J. Mater. Chem. A*, 2015, **3**, 10158–10173.
15 J. Jiang, Y. Y. Li, J. P. Liu, X. T. Huang, C. Z. Yuan and X. W. Lou, *Adv. Mater.*, 2012, **24**, 5166–5180.
16 X. H. Xia, J. P. Tu, Y. Q. Zhang, X. L. Wang, C. D. Gu, X. B. Zhao and H. J. Fan, *ACS Nano*, 2012, **6**, 5531–5538.
17 G. Q. Zhang, H. B. Wu, H. E. Hoster, M. B. Chan-Park and X. W. Lou, *Energy Environ. Sci.*, 2012, **5**, 9453–9456.
18 R. B. Rakhi, W. Chen, D. Cha and H. N. Alshareef, *Nano Lett.*, 2012, **12**, 2559–2567.
19 J. W. Xiao, L. Wan, S. H. Yang, F. Xiao and S. Wang, *Nano Lett.*, 2014, **14**, 831–838.
20 X. H. Lu, G. M. Wang, T. Zhai, M. H. Yu, S. L. Xie, Y. C. Ling, C. L. Liang, Y. X. Tong and Y. Li, *Nano Lett.*, 2012, **12**, 5376–5381.
21 L. Liu, Y. Yu, C. Yan, K. Li and Z. Zheng, *Nat. Commun.*, 2015, **6**, 7260.
22 H. J. Feng, S. H. Tao, X. Y. Zhang, J. Li, Z. H. Liu and X. Fan, *Chem. Commun.*, 2014, **50**, 3509–3511.
23 N. N. Zhang, J. Chen, Y. Huang, W. W. Guo, J. Yang, J. Du, X. Fan and C. Y. Tao, *Adv. Mater.*, 2016, **28**, 263–269.
24 K. F. Chen and D. F. Xue, *Funct. Mater. Lett.*, 2014, **7**, 1430001.
25 K. F. Chen and D. F. Xue, *J. Phys. Chem. C*, 2013, **117**, 22576–22583.
26 X. J. Zhang, W. H. Shi, J. X. Zhu, D. J. Kharistal, W. Y. Zhao, B. S. Lalia, H. H. Hng and Q. Y. Yan, *ACS Nano*, 2011, **5**, 2013–2019.
27 K. V. Gurav, U. M. Patil, S. W. Shin, G. L. Agawane, M. P. Suryawanshi, S. M. Pawar, P. S. Patil, C. D. Lokhande and J. H. Kim, *J. Alloys Compd.*, 2013, **573**, 27–31.
28 P. P. Xu, K. Ye, M. M. Du, J. J. Liu, K. Cheng, J. L. Yin, G. L. Wang and D. X. Cao, *RSC Adv.*, 2015, **5**, 36656–36664.
29 L. Chen, Y. Zhang, P. L. Zhu, F. R. Zhou, W. J. Zeng, D. D. Lu, R. Sun and C. P. Wong, *Sci. Rep.*, 2015, **5**, 9672.
30 Y. M. Chen, X. Y. Li, X. Y. Zhou, H. M. Yao, H. T. Huang, Y. W. Mai and L. M. Zhou, *Energy Environ. Sci.*, 2014, **7**, 2689–2696.
31 R. X. Wang, X. M. Tao, Y. Wang, G. F. Wang and S. M. Shang, *Surf. Coat. Technol.*, 2010, **204**, 1206–1210.
32 V. Augustyn, P. Simon and B. Dunn, *Energy Environ. Sci.*, 2014, **7**, 1597–1614.
33 J. L. Liu, J. Wang, Z. L. Ku, H. H. Wang, S. Chen, L. L. Zhang, J. Y. Lin and Z. X. Shen, *ACS Nano*, 2016, **10**, 1007–1016.
34 V. Barranco, M. A. Lillo-Rodenas, A. Linares-Solano, A. Oya, F. Pico, J. Ibañez, F. Agullo-Rueda, J. M. Amarilla and J. M. Rojo, *J. Phys. Chem. C*, 2010, **114**, 10302–10307.
35 J. L. Liu, L. L. Zhang, H. B. Wu, J. Y. Lin, Z. X. Shen and X. W. Lou, *Energy Environ. Sci.*, 2014, **7**, 3709–3719.
36 G. M. Wang, H. Y. Wang, X. H. Lu, Y. C. Ling, M. H. Yu, T. Zhai, Y. X. Tong and Y. Li, *Adv. Mater.*, 2014, **26**, 2676–2682.
37 Y. P. Fu, X. Cai, H. W. Wu, Z. B. Lv, S. C. Hou, M. Peng, X. Yu and D. C. Zou, *Adv.Mater.*, 2012, **24**, 5713–5718.
38 J. Ren, W. Y. Bai, G. Z. Guan, Y. Zhang and H. S. Peng, *Adv. Mater.*, 2013, **25**, 5965–5970.
39 Y. N. Meng, Y. Zhao, C. G. Hu, H. H. Cheng, Y. Hu, Z. P. Zhang, G. Q. Shi and L. T. Qu, *Adv. Mater.*, 2013, **25**, 2326–2331.
40 V. T. Le, H. Kim, A. Ghosh, J. Kim, J. Chang, Q. A. Vu, D. T. Pham, J. H. Lee, S. W. Kim and Y. H. Lee, *ACS Nano*, 2013, **7**, 5940–5947.
41 Y. P. Fu, H. W. Wu, S. Y. Ye, X. Cai, X. Yu, S. C. Hou, H. Kafafy and D. C. Zou, *Energy Environ. Sci.*, 2013, **6**, 805–812.
42 M. Jayalakshmi and K. Balasubramanian, *Int. J. Electrochem. Sci.*, 2008, **3**, 1277–1287.